18th Australasian Fluid Mechanics Conference
Launceston, Australia
3-7 December 2012

Meandering Riblets Targeting Spanwise Spatial Oscillation of Turbulent Boundary Layer

K. X. Oh, B. Nugroho, N. Hutchins, J. P. Monty

Department of Mechanical Engineering
The University of Melbourne, Victoria, 3010, AUSTRALIA

Abstract

Turbulent boundary layers are investigated over meandering and straight riblets for a range of Reynolds numbers ($1400 < Re_\tau < 2800$). This work is motivated by previous studies of riblets and temporal spanwise oscillation that have both demonstrated viscous drag reduction in turbulent boundary layers. Mean velocity profiles acquired over these surfaces are regression fitted to the canonical profile using the roughness modified Clauser and velocity defect plots to determine the friction velocity U_τ and virtual origin z_0. This method for meandering riblets is inconclusive with the variation of U_τ and z_0 within the margin of experimental error. Moreover, the velocity profile over the meandering riblets seems to challenge the applicability of the universal outer form. For both meandering and straight riblets, robust modifications are observed in the turbulence intensity of the streamwise velocity signal (u') and pre-multiplied energy spectrum ($k_x\phi_{uu}$). A reduction in the near-wall peak of u' is observed for both riblet cases compared to the smooth wall. This is more pronounced for the meandering case. The measured energy spectra in the near-wall region suggest that for the riblet cases the energy contribution from scales consistent with the near-wall cycle are reduced. This is again more pronounced for the meandering case. Finally, it is noted that the meandering riblets cause increased magnitude (compared to smooth) of the large-scale turbulent energy in the outer part of the boundary layer ($z/\delta \approx 0.07$), suggesting that these surfaces modify the largest scale coherent motions residing in the log and wake regions of the flow.

Introduction

Straight riblets with varying cross-sectional geometries have been researched extensively based on their ability to reduce the skin friction drag penalty of turbulent boundary layers. [8] provides a review of research on straight riblets. Riblets of different cross sectional geometries have been thoroughly investigated by [1]. Riblets of spacing $s^+ = 15$ to 25 and with spacing to height ratio $s/h \approx 0.5$ yield optimal drag reductions (here s is the spanwise peak-to-peak spacing of the riblets, h is the peak-to-trough riblet height and the superscript $+$ represents scaling with viscous units, i.e. $s^+ = sU_\tau/\nu$ where U_τ is the friction velocity and ν is the kinematic viscosity). Active perturbations with spanwise oscillation of wall flows have also been studied for flow control and can yield a drag reduction as high as 40% in turbulent boundary layer flows as reported by [7] and [10]. However, an energy input is required for the wall oscillation, which when accounted for reduces the net energy savings. The promising aspects of spanwise oscillation for drag reduction coupled with the impracticality of wall oscillations in real world applications has instigated the study of meandering riblets to passively induce spanwise oscillations of turbulent boundary layers. A previous LES study on meandering riblets at $Re_\tau = 180$ has been conducted by [9] who obtained a drag reduction of 7.4% (a reported 2% improvement over conventional straight riblets). The work reported in this paper focuses on an experimental study of meandering riblets at moderately high Reynolds number.

Method

Boundary layer profiles over the meandering and straight riblet tiles are acquired at Reynolds number Re_τ= 1400, 2000 and 2800 (where Re_τ is the friction Reynolds number defined as $Re_\tau = \delta U_\tau/\nu$ where δ is the boundary layer thickness based on 99.5% of freestream velocity). A single-normal 5 μm hot-wire is used for the traverse, located 4 m downstream of the tripped inlet to the working section. The hotwire is operated in constnat temperature mode using an in-house Melbourne University constant temperature anemometer (MUCTA). The riblets tiles are sized at 500 mm $\times$300 mm, with experiments conducted over a test surface consisting of 8 tiles covering a central strip of length 4 m in the tunnel. Figure 1 shows the meandering riblet geometry used in the current investigation. Throughout this paper x, y and z refer to the streamwise, spanwise and wall-normal directions respectively. The associated velocity components are u, v and w. Capitalised variables and over bars denote time-averaged values, and lowercase denotes fluctuating quantities.

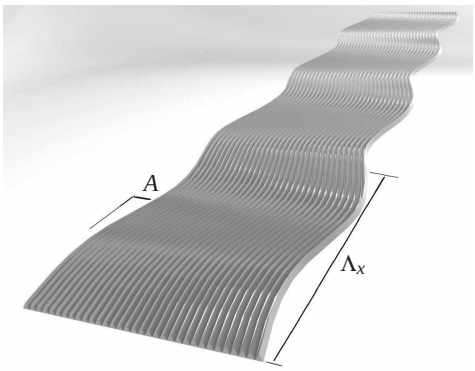

Figure 1: Schematic of meandering riblets.

Meandering Riblets

Aside from the riblet cross-sectional geometries (h and s) an additional two aspects of the meandering riblets are to be determined — the streamwise wavelength Λ_x and amplitude A of the meandering arrangement, as illustrated in Figure 1. Most present literature on spanwise wall oscillations focus on temporal forcing of the oscillating wall. However, [10] performed a DNS study investigating spatial spanwise forcing functions which were reported to yield similar optimal drag reductions. They reported a maximum drag reduction of 52% with a streamwise forcing wavelength $\Lambda_x^+ = 1250$ and spanwise velocity amplitude $V^+ = 20$. Our initial experiment focuses on $Re_\tau = 2000$, where the meandering riblets were designed with $\Lambda_x^+ = 1250$ and a streamwise wave amplitude $A^+ = 55$ at this speed. Note that A here is a length scale, whereas V as reported in [10] is a velocity scale. From [10], their results suggests that higher V yields higher drag reduction, with no obvious limiting bound as far as drag reduction is concerned. We consult [4] whose results suggest that a 15° riblet yaw angle is a limiting bound for drag reduction. The amplitude of the meandering riblets in this study is hence limited such that the maximum yaw angle from

the streamwise direction (at the position $\Lambda/2$ of a sine wave) is $\theta = 15^\circ$. With a maximum yaw angle of $\theta = 15^\circ$ and a streamwise wavelength of $\Lambda_x = 1250$, we use equation (1) to obtain the approximate maximum spanwise displacement (A^+) of the meandering riblets.

$$A^+ = \frac{\Lambda_x^+ tan(\theta)}{2\pi} \quad (1)$$

Assuming a convection velocity at the crest of the riblets of approximately $U_c^+ \approx 10$, and assuming that the riblets redirect the flow at the meandering angle, we estimate that $V^+ \approx 3$ (which [10] shows for $\Lambda_x^+ = 1250$ could give up to 15% drag reductions). The riblets are of 60° triangular cross-section with height and spacing set at $h^+ = 18$ and $s^+ = 25$, which was inherited from previous studies of converging-diverging riblet geometries conducted using the same facilities (see [6] for description of the riblet cross-section geometry).

Straight Riblets

Straight (non-meandering) riblets were also studied to serve as a baseline case to isolate the effect of the meandering arrangement on the boundary layer profiles. The riblets are of scallop / semi-circular shaped cross section with height and spacing set at $h^+ = 9$ and $s^+ = 18$ (which were determined from the optimum straight riblet geometries for drag reduction as reported by [1]). Similar manufacturing processes, materials and experimental set-up were adopted as with the meandering riblets.

Table 1 tabulates the riblet cross-sectional geometries and meandering parameters corresponding to the different Reynolds number experiments. It should be noted that due to difficulties in determining the friction velocity U_τ over the ribbed surfaces, all dimensions are here non-dimensionalised using the smooth wall of U_τ at that particular Reynolds number.

	$Re_\tau = 1400$	$Re_\tau = 2000$	$Re_\tau = 2800$
U_∞ (ms^{-1})	10	15	20
x (m)	4	4	4
Meandering	60° tip triangular cross-section		
h_m^+	12.5	18.0	24.0
s_m^+	17.0	25.0	32.5
Λ_x^+	880	1250	1680
A^+	37.5	55.0	72.0
Straight	scallop/semi circular cross section		
h_s^+	6.0	9.0	12.0
s_s^+	12.0	18.0	24.0

Table 1: Geometries of riblets in wall units. Subscripts *m* and *s* corresponds to meandering and straight riblets accordingly.

Determining the wall-normal position

Experiments are conducted in a zero pressure gradient wind-tunnel with a working section of 0.94 m ×0.375 m cross-section and length 6.7 m. The hot-wire probe is placed 4 m downstream from the tripped inlet and is mounted to a cylindrical sting that is attached to a stepper motor driven vertical traverse. A vertically traversing microscope is used to position the probe as close as 0.25 mm from the smooth wall or the riblet tips for the start of the traverse. A camera located outside of the tunnel, positioned 0.5 m away from the probe in the spanwise direction is used to capture any movement of the probe after the tunnel is switched on. Such movements would include any deflection of the cylindrical sting due to aerodynamic loading and also any deflection of the wall of the tunnel due to the tunnel being at positive pressure when in operation. High-resolution images of the hot-wire probe are taken before and after the tunnel is switched on, and any movements are approximated using cross-correlation of the images. We estimate (based on the resolution of the images and repeatability) that an accuracy of $50\mu m$ can be obtained with this technique. The accuracy of the system can be verified by comparing the measured smooth wall mean velocity profile to that obtained from direct numerical simulation (DNS).

Results

For this section, boundary layer profiles over the meandering and straight riblets are compared with the smooth wall case in several aspects including mean velocity profile, turbulence intensity and premultiplied energy spectrum.

Mean Velocity and Turbulence Intensity

To investigate the presence of drag reduction, we attempt to fit both the smooth and riblet mean velocity profiles to a canonical turbulent boundary layer profile. For the riblet case, we use the modified Clauser technique [3], assuming a universal gradient in the logarithmic region with a modified or adjusted intercept ΔU^+. This modified profile is given in equation (2).

$$U^+(z) = \frac{1}{\kappa} ln(\hat{z}^+) + A - \Delta U^+ \quad (2)$$

An upward shift in the mean velocity profile (a negative ΔU^+ or negative roughness function) indicates a drag reduction. Here $U^+ = U/U_\tau$ and $\hat{z}^+ = \hat{z}U_\tau/\nu$ where $\hat{z}$ is the wall-normal distance from the virtual origin ($\hat{z} = z - z_0$, where z is the measured wall-normal distance from the trough of the riblet geometry and z_0 is an unknown roughness offset.) The universal logarithmic constants used here are $\kappa = 0.41$ and $A = 5.0$.

The measured smooth wall profiles at all three Reynolds numbers are first fitted to the logarithmic region equation to obtain an estimate for the friction velocity U_τ (the Clauser technique [3]). For the riblet profiles, Choi [2] suggests that the mean velocity profile over straight riblets obeys the universal logarithmic form, where it was reported that the Clauser plot yields a $-\Delta U^+$ (upward shift) indicating drag reduction. This assumption was adopted and applied here. The data are fitted to the modified Clauser equation given in equation (2). This equation alone is difficult to fit to, since there are three unknowns (U_τ, z_0 and ΔU^+). There are multiple combinations of these three variables that give a good fit of the data to equation (2), and thus a unique solution is not obvious. To solve this, we also make use of the velocity defect plot for the outer region where $z^+ \geq 100$,

$$\frac{U - U_\infty}{U_\tau} = f\left(\frac{\hat{z}}{\delta}\right) \quad (3)$$

Outer layer similarity would suggest that when scaled in this manner, the smooth and rough (riblet) data should collapse. Equation (3) offers a further check of the possible combinations of U_τ and z_0 suggested from equation (2), and regression fitting will yield the most likely candidate combination.

Ultimately, the above methodology of fitting to determine U_τ for the riblet surfaces has not yielded conclusive and repeatable results, with any measured change of U_τ within the margin of experimental error. For the meandering riblets, we observe that the assumption of outer layer similarity (and hence the use of the velocity defect plot) is not entirely justified, with some differences observed in the wake profile for the meandering case. Without this assumption, it is impossible for us accurately determine U_τ with the current experimental set-up. A drag balance will ultimately need to implemented in future studies to obtain a direct measurement of U_τ. As a preliminary summary, and to the best we can determine with the above methodology, we

note that meandering riblets appear to behave as a marginally transionally rough surface, i.e. a possible $1-2\%$ drag increase compared to the smooth wall. Straight riblets, on the other hand, tend to yield a slight drag reduction (as would be expected from the wealth of literature on these surfaces).

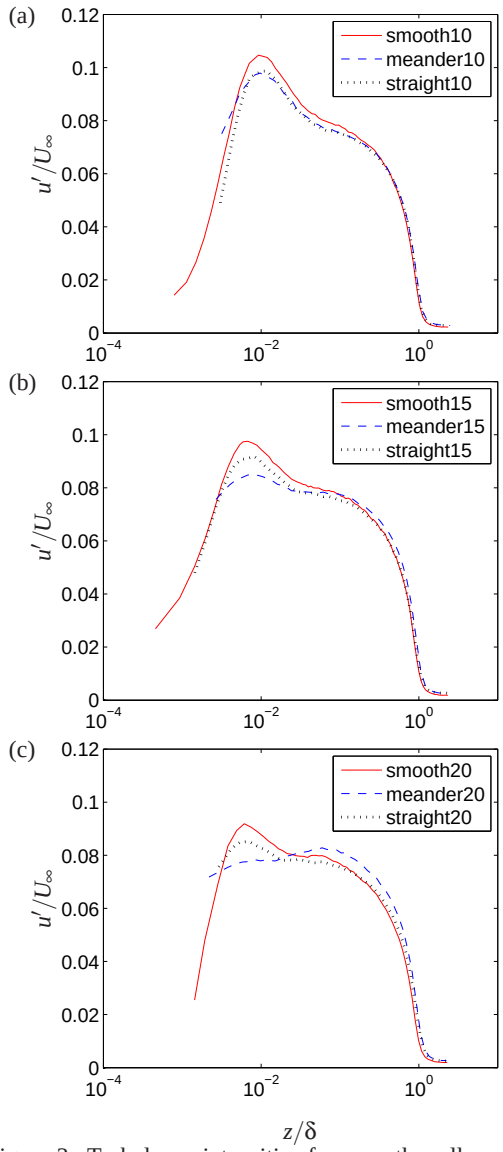

Figure 2: Turbulence intensities for smooth wall, meandering and straight riblet surfaces at (a) $Re_\tau = 1400$, (b) $Re_\tau = 2000$ and (c) $Re_\tau = 2800$.

In the absence of accurate and reliable estimates of U_τ, we here we present the turbulence statistics normalized by the freestream velocity U_∞ and the boundary layer thickness δ so that comparison can be made between the flow over the smooth surface and the straight and meandering riblet cases. Figure 2 shows the root-mean-squared turbulence intensity of streamwise velocity fluctuations (u') for the 3 different Reynolds number ($Re_\tau = 1400$, 2000 and 2800 corresponding to freestream velocity $U_\infty = 10, 15$ and 20 ms^{-1}). It is clear from figure 2 that the riblets attenuate the near-wall peak of the turbulence intensity profile, and the effect is more significant for the meandering riblets as compared to the straight riblets as the Reynolds number (and hence h^+ of the riblets) increases. At $Re_\tau = 2800$ the near-wall peak intensity for the meandering riblets is attenuated to such an extent that the peak is absent altogether. In making this observation however, it is important to remember that the meandering riblets are of slightly larger riblet height h^+ and spacing s^+ than the straight riblets.

Further from the surface, the intensity over the meandering riblets starts to exceed that of smooth wall for $z/\delta \gtrsim 0.02$ or $z^+ \gtrsim 55$, with a peak excess energy occurring at $z/\delta \approx 0.2$ and finally converging with the smooth wall profile at the edge of boundary layer. This might suggest that some of the energy from the near-wall region (below $z/\delta = 0.02$) has been shifted to the outer region by the meandering riblet pattern. In fact, this effect is also observable (though to a lesser extent) at $Re_\tau = 2000$. This change in shape of the turbulence intensity profiles further verifies our earlier observation that the meandering riblets alter the boundary layer profiles such that the assumption of outer-layer similarity is no longer satisfied.

Premultiplied Energy Spectrum

Figure 3 presents the pre-multiplied energy spectra $k_x\phi_{uu}$ (where k_x is the streamwise wavenumber and ϕ_{uu} is the energy spectrum of the streamwise velocity fluctuations) as function of streamwise wavelength λ_x ($= 2\pi/k_x$) and distance from the wall z. The spectra maps are scaled with freestream velocity U_∞ and the boundary layer thickness δ for comparison to the smooth wall. In figure 3 we present the pre-multiplied energy spectrum throughout the boundary layer for Reynolds number $Re_\tau = 2000$ (top row plots *a*, *b*, *c*) and 2800 (bottom row plots *d*, *e*, *f*). The results for $Re_\tau = 1400$ are not presented here since there is very little observable difference between the smooth and the riblet cases (the small viscous-scaled riblet height at this Reynolds number is insufficient to significantly perturb the energy profile). Figure 3 (*a*) and (*d*) show the smooth wall spectra, while (*b*) and (*e*) and plots (*c*) and (*f*) show the meandering and straight riblet spectra respectively.

In Figure 3 (*b*) and (*e*), the horizontal lines plotted on top of the spectra contours represent the scale of the normalized streamwise sinusoidal wavelength Λ_x/δ of the meandering riblet pattern. We can clearly see that close to the wall ($z/\delta \lesssim 0.02$) at both Reynolds numbers the meandering riblets have significantly reduced the magnitude of the energy contributed by structures of scale $\lambda_x \geq \Lambda_x$ when compared to the smooth wall. Equally significantly, we also notice in the meandering case, for the highest Reynolds number, that the magnitude of large-scale energy at the outer peak (centered around $z/\delta = 0.07$ and $\lambda_x/\delta = 6$) seems to be greater in magnitude over the meandering riblets (as compared to both the smooth wall and the straight riblets). This outer peak is typically associated with the very large scale motions or 'superstructures' [5], and the implication here seems to be that the meandering riblet geometry is somehow interacting with these very large-scale coherent motions in a manner that increases the overall turbulent energy at this scale. The straight riblets exhibit no discernable change in energy at this outer peak location. This finding is consistent with the turbulent intensity results of figure 2, and confirms that the increased broadband intensity for $z/\delta \gtrsim 0.02$ is due to increased energy in the very long wavelengths.

In general we observe that at higher Reynolds number ($Re_\tau = 2800$) the noted effects of the meandering riblets are more pronounced on the energy spectra. At this Reynolds number, the height and spacing of the meandering riblets are larger in wall units, suggesting that a plausible passive periodic forcing is imposed on the boundary layer due to the meandering waves of the riblet pattern. In the near-wall region, the fact that the meandering riblets attenuate energy contributions from scales greater that Λ_x could be interpreted as the result of a spatial periodic forcing and assumed to be a direct consequence of the meandering wavelength. However, an equally plausible sug-

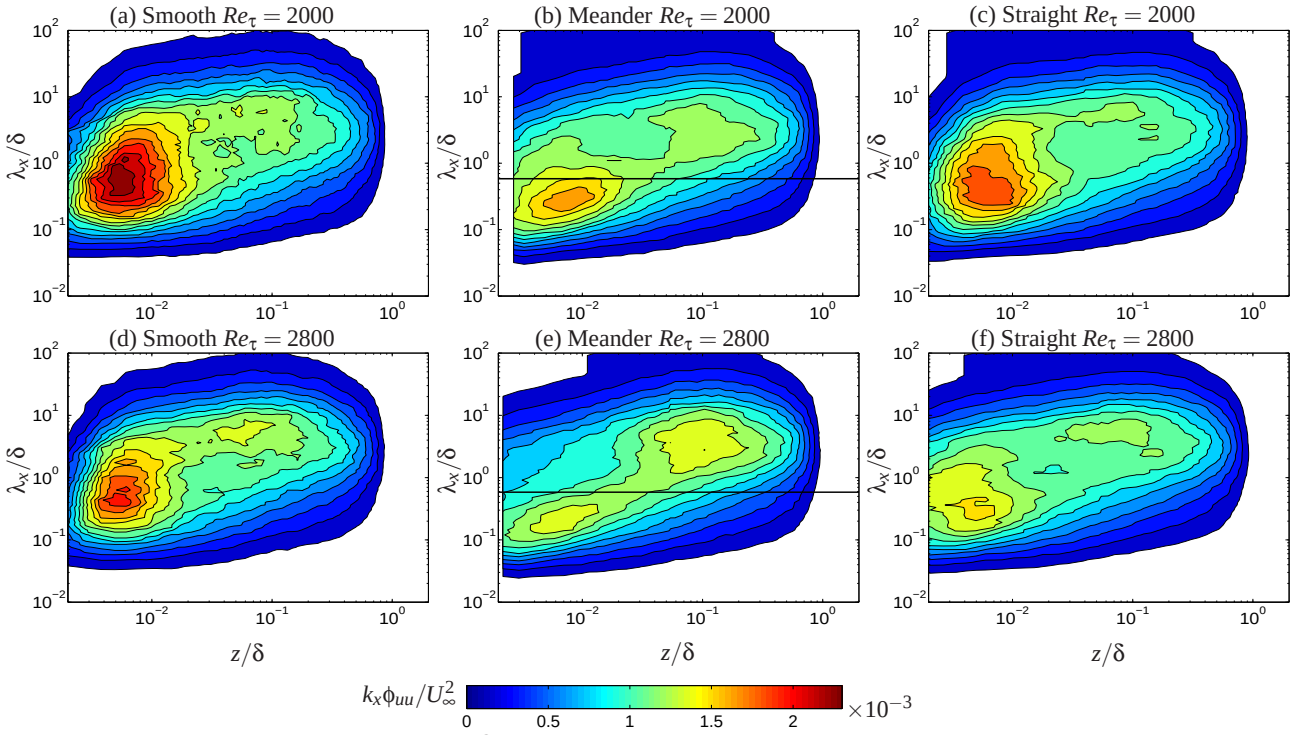

Figure 3: Premultiplied energy spectra $k_x\phi_{uu}/U_\infty^2$ contours for (a,d) smooth wall (b,e) meandering and (c,f) straight riblets at two Reynolds number as indicated, plotted as a function of wall normal position z/δ and energetic streamwise length scale λ_x/δ.

gestion would be that the meandering riblets have substantially reduced the energy from the near-wall cycle, which has been shown to have a dominant wavelength ($\lambda_x = 1000$)[5] which is very close to the meandering wavelength (Λ_x) of the surface used here. Further tests with vastly different meandering wavelengths could potentially resolve this question.

Conclusions

The meandering riblets were found to significantly perturb the turbulence intensity and premultiplied energy spectrum profiles at high Reynolds number $Re_\tau = 2800$, where the riblet grooves are the largest in viscous wall units. The near-wall peak of the turbulence intensity profile is found to be heavily attenuated, while an increase in the intensity is found in the outer region. This result is further investigated through the premultiplied energy spectra. The near-wall energy contribution from structures of scales greater than the meandering riblet wavelength have been significantly reduced. This could be a result of forcing at the scale of the meandering wavelength, or could be equally well be indicative of a more general disruption of the near-wall cycle. More intriguingly, the outer energetic peak is significantly strengthened for the meandering riblets, patrticularly for the highest Reynolds number. This peak is typically associated with the very largest scale motions (or superstructures), and implies that the meandering pattern, despite the very small roughness height, is somehow able to strengthen coherent motions that exist in the log and wake regions of the boundary layer.

Acknowledgements

The authors gratefully acknowledge support from the Australian Research Council.

References

[1] Bechert, D. W., Bruse, M., Hage, W., der Hoeven, J. G. T. V. and Hoppe, G., Experiemnts on drag-reducing surfaces and their optimization with an adjustable geometry, *J. Fluid Mech.*, **338**, 1997, 59–87.

[2] Choi, K.-S., Near-wall structure of a turbulent boundary layer with riblets, *J. Fluid Mech.*, **208**, 1989, 417–458.

[3] Clauser, F. H., The turbulent boundary layer, *Adv. Applied Mech*, **4**, 1956, 1–51.

[4] Dean, B. and Bhushan, B., Shark-skin surfaces for fluid-drag reduction in turbulent flow: A review, *Phil. Trans. R. Soc. A*, **368**, 2010, 4775–4806.

[5] Hutchins, N. and Marusic, I., Large-scale influences in near-wall turbulence, *Phil. Trans. R. Soc. A*, **365**, 2007, 647–664.

[6] Hutchins, N., Nugroho, B. and Monty, J. P., Large-scale secondary flows in a turbulent boundary layer caused by highly ordered and directional surface roughness., in *ETMM9: 9th International ERCOFTAC Symposium on Engineering Turbulence Modelling and Measurements*, 2012.

[7] Jung, W. J., Mangiavacchi, N. and Akhavan, R., Suppression of turbulence in wall-bounded flows by high-frequency spanwise oscillation, *Phys. Fluids*, **4**, 1992, 1605.

[8] Lee, S.-J. and Lee, S.-H., Flow field analysis of a turbulent boundary layer over a riblet surface, *Exp. Fluids*, **30**, 2001, 153–166.

[9] Peet, Y., Sagaut, P. and Charron, Y., Turbulent drag reduction using sinusoidal riblets with triangular cross-section, *AIAA-paper*, aIAA-2008-3745.

[10] Viotti, C., Quadrio, M. and Luchini, P., Streamwise oscillation of spanwise velocity at the wall of a channel for turbulent drag reduction, *Phys. Fluids*, **21**, 2009, 115109.